Philosophical Magazine

ISSN: 1478-6435 (Print) 1478-6443 (Online) Journal homepage: https://www.tandfonline.com/loi/tphm20

Polyethylene glycol-assisted growth of Cu_2SnS_3 promising absorbers for thin film solar cell applications

S. Kahraman, S. Çetinkaya, S. Yaşar & İ. Bilican

To cite this article: S. Kahraman, S. Çetinkaya, S. Yaşar & İ. Bilican (2014) Polyethylene glycol-assisted growth of Cu_2SnS_3 promising absorbers for thin film solar cell applications, Philosophical Magazine, 94:27, 3149-3161, DOI: 10.1080/14786435.2014.952257

To link to this article: https://doi.org/10.1080/14786435.2014.952257

Published online: 01 Sep 2014.

Submit your article to this journal

Article views: 204

View related articles

View Crossmark data

Citing articles: 10 View citing articles

Full Terms & Conditions of access and use can be found at
https://www.tandfonline.com/action/journalInformation?journalCode=tphm20

Philosophical Magazine, 2014
Vol. 94, No. 27, 3149–3161, http://dx.doi.org/10.1080/14786435.2014.952257

Taylor & Francis
Taylor & Francis Group

Polyethylene glycol-assisted growth of Cu_2SnS_3 promising absorbers for thin film solar cell applications

S. Kahraman[a]*, S. Çetinkaya[b], S. Yaşar[b] and İ. Bilican[c]

[a]*Faculty of Technology, Department of Metallurgy and Material Engineering, Mustafa Kemal University, 31034 Hatay, Turkey;* [b]*Semiconductor Research Laboratory/Group, Physics Department, Mustafa Kemal University, Hatay, Turkey;* [c]*Scientific and Technological Applications and Research Center, Aksaray University, Aksaray, Turkey*

(*Received 26 May 2014; accepted 3 August 2014*)

In this paper, we report, for the first time, the results of the polyethylene glycol- (PEG) assisted preparation and characterization of high-quality and well-crystallized Cu_2SnS_3 (CTS) thin films obtained using sol–gel spin-coating method and a subsequent annealing in a sulphur atmosphere. Structural, morphological, compositional, electrical and optical investigations were carried out. The X-ray diffraction patterns of the samples proved the polycrystalline nature and preferred crystallization of the films. No peak referring to other binary or ternary phases were detected in the patterns. The intensity of the preferred orientation and crystallite size of the films increased with increasing PEG content. This trend yielded an improvement in photo-transient currents of the PEG-assisted growth of CTS films. The scanning electron microscopy images revealed that the CTS films have continuous, dense and agglomeration-like morphology. Through energy dispersive X-ray spectroscopy studies, it has been deduced that the samples consist of Cu, Sn and S of which atomic percentages were consistent with Cu/Sn and S/metal initial ratios. The agglomerated morphology of the samples has been attributed to increasing PEG content. A remarkable enhancement was observed in photo-transient currents of p-n junction of the produced films along with increasing PEG content. Through resistivity-temperature measurements, three impurity level electrical activation energy values for each film were found. Optical band gap values of the films were estimated via absorbance-wavelength behaviours and decreased with increasing PEG content. It has been revealed that PEG-assisted growth of CTS thin films is a promising way to improve its photovoltaic characteristics.

Keywords: sulphides; thin films; solution growth; photovoltaics

1. Introduction

As a renewable energy source, solar energy is believed to be one of the greenest ways in obtaining energy. Recently, there has been a great deal of interest in the production of photovoltaic modules due to rapid increase in demand for renewable energy. However, efforts are still needed to make photovoltaics cost-competitive over other established technologies for energy production [1]. The research on thin film solar cells

*Corresponding author. Email: skahraman@mku.edu.tr

© 2014 Taylor & Francis

based on compound semiconductor absorber layers has mainly concentrated on Cu(In, Ga)(S,Se)$_2$ (CIGS), CdTe and $Cu_2ZnSn(S/Se)_4$ (CZTS). In spite of several advantages, these compound absorber materials have a complex structure and require very controlled growth conditions. Compared to these compounds, there are other ternary Cu–Sn–S or Cu–In–S systems which have fewer elements and less complexity. Recently, the group of these chalcocuprites has attracted much attention because of their important potential applications in photovoltaic cells [2,3] and lithium-ion batteries [4,5]. There has been a great demand for achieving indium-free photovoltaic materials because of high cost and scarcity of indium, and its wide usage in current display technology.

Cu–Sn–S compounds are promising absorber materials for the production of cheaper large-scale thin film solar cells due to the abundancy of tin in the earth's crust [6–11]. The mineral form of Cu_2SnS_3 (CTS) was found firstly by Kovalenker et al. [12]. The photovoltaic behaviour of CTS thin films was reported for the first time by Kuku and Fakolujo [13]. Resulting from their In-free composition, semiconducting copper tin sulphides such as Cu_2SnS_3, Cu_3SnS_4 and $Cu_4Sn_7S_{16}$ could have an important role in the near future [14]. The CTS compound with cubic polymorph can be obtained at temperatures higher than 775 °C while mono-clinic, triclinic as well as the tetragonal phases can be more probably at low temperatures (<775 °C) [15–18]. CTS is one of the most promising materials which can be used in solar cells due to its band gap close to that expected for photovoltaic conversion [18]. An absorption coefficient of 10^4 cm^{-1}, an electrical conductivity of 10 Ω^{-1} cm^{-1}, a hole mobility of 80 cm^2 V^{-1}s^{-1} and a hole concentration of 10^{18} cm^{-3} have been measured for a CTS phase [6]. Depending on the type of crystal structure of this compound, its band gap energy varies between 0.93 and 1.51 eV [19].

Several studies on CTS have been reported [2,3,7–10,12,14,16–24]. Su et al. prepared (Cu,Sn)S thin films by annealing three precursor films and they improved the growth rate of the deposition via ion exchange [7]. Koike et al. [8] fabricated Mo/Cu_2SnS_3/CdS/ZnO: Al/Al structure from the CTS thin films prepared by sulphurizing Cu–Sn precursors deposited by co-electrodeposition. They achieved a conversion efficiency of 2.84% from the films with Cu/Sn ≤ 2. Avellaneda et al. [9] obtained Cu_2SnS_3 thin films by sequential chemical deposition of copper sulphide and tin sulphide. Bouaziz et al. [14] reported Cu_2SnS_3 thin films from sandwich layers of SnS_2 and Cu_xS obtained using the spray pyrolysis technique. They found that the material is p-type with direct transition band gap of 1.15 eV and high absorption coefficient of ~10^4 cm^{-1}. The basic properties of tetragonal CTS and rhombohedral $Cu_4Sn_7S_{16}$ bulk crystals were studied by Chen et al. [16]. Onoda et al. [17] produced CTS crystals by means of a conventional solid-state reaction. Bouaziz et al. [18] achieved CTS thin film by annealing, in sulphur atmosphere, of sequentially deposited copper/tin sandwich layers. Fernandes et al. [19,20] reported the results of the growth and characterization of Cu_2SnS_3, Cu_3SnS_4, ZnS and Sn_xS_y thin films obtained via sulphurization of dc magnetron-sputtered metallic precursor layers. Chen et al. [21] studied photovoltaic properties of Cu_2SnS_3 films synthesized by means of a stoichiometric ball-milling process. Nanocrystalline CTS at synthetic conditions of low temperature (<180 °C) was reported by Li et al. [18]. Amlouk et al. [23] reported deposition of $CuIn_5S_8$ and CTS thin films using annealing in sulphur atmosphere at 550 °C during evaporation of copper on In_2S_3- and SnS_2-sprayed thin

films, respectively. Li et al. [24] prepared graphene/CTS quantum dot composites using a hydrothermal method. The results showed that the size of the CTS quantum dots in the composites was less than that of the separately grown CTS quantum dots. Dahman et al. [25] prepared Cu_2SnS_3 films for the first time by sol–gel spin-coating route on glass substrate. They found that the films have tetragonal phase with (1 1 2) preferential orientation and were composed of 5 nm-sized grains.

As discussed above, a variety of methods have been reported for the preparation of CTS. Among them, chemical solution deposition methods have several advantages, very important one being that a variety of thin films can be grown at low temperatures using cheap manufacturing equipment. The sol–gel method is a very simple and low-cost process based on hydrolysis and poly-condensation reactions. Sulphide films can be directly obtained by sulphurizing oxyhydrate precursors. Moreover, sol–gel process may also allow more precise control of film thickness, particle size and porosity by adjusting different parameters such as, sol concentration, spin speed, annealing temperature and so on [26]. To the best of our knowledge, only one attempt has been made to manufacture CTS thin films via sol–gel spin-coating method [25]. In order to improve the characteristics of Cu–Sn–S systems, many investigations should be carried out. It is well known that the characteristics of functional materials can be tuned using additives. Generally, additives used in chemical growth methods control the surface morphology, crystalline structure and refine the grain size [27]. The presence of additives also influences physical and mechanical properties such as grain size, porosity, brightness, internal stress, pitting, corrosion behaviour and even chemical composition. As an additive material, polyethylene glycol (PEG) considerably enhances the surface morphology and affects the growth dynamic of particle growth as well as it has been used as a binder and pore-forming agent in TiO_2-based dye synthesized solar cells [28–35]. Rahman et al. [26] added 40% PEG by weight in TiO_2 precursor solution and found smooth, crack-free and highly porous film with high cell efficiency. Fan et al. [32] attempted to control the microstructure of TiO_2 coating with PEG in different contents. They achieved a conversion efficiency of 7.1% using a composite TiO_2 powder containing 41.2% PEG. Pradubsang et al. [33] studied the effects of PEG on photo electrode porosity to reduce the formation of cracks which occurs during sintering. They found that short-circuit photocurrent density increased with increasing PEG amount, and the photo electrode made from paste with 60% PEG showed 4.69% conversion efficiency. Physical characteristics of Cu–Sn–S systems may be improved by assistance of PEG. The role of PEG in CTS deposition process has not been studied yet. Thus, it is of interest to us to investigate the effects of PEG on morphology, crystallographic structure, electrical properties and photovoltaic response of the CTS thin films.

Here, we report, for the first time, the results of the PEG-assisted preparation and characterization of high-quality and well-crystallized CTS thin films obtained using sol–gel spin-coating method and a subsequent annealing in a sulphur atmosphere. The physical characteristics of the films were brought out by means of X-ray diffraction (XRD), scanning electron microscopy, energy-dispersive X-ray spectroscopy (EDXS), UV–visible spectroscopy, photo-transient current measurements and electrical resistivity-temperature behaviour.

2. Experimental

It has been reported that copper tends to make secondary phases in Cu–Sn–S compounds. It should be grown under Cu-poor conditions to prevent $Cu_{2-x}S$ or other binary/ternary phases and to improve the performance of the film. Conversion efficiencies of 2.84 and 2.54% were obtained in a CTS-based solar cell with Cu/Sn ratios of 1.88 and 1.86, respectively [8,11]. Cu-poor conditions enhance the formation of Cu vacancies, which give rise to shallow acceptors [36]. Another reason to use copper-poor composition is some Sn loss which occurs during the sulphurization process, mainly in the form of SnS [19]. In this work, therefore, for the deposition of CTS thin films, we prepared the starting solutions with a Cu/Sn ratio of 1.80. The solutions were prepared by dissolving copper (II) acetate monohydrate (0.9 M, 98+%), tin (II) cloride (0.5 M, 98%) from Sigma Aldrich and thiourea as a sulphur source (0.2 M, 99.0+% from Sigma Aldrich), into 2-methoxyethanol (99.8% from Sigma Aldrich) and 25 µl of diethanolamine was added slowly into each solution as a stabilizer while stirring. Then 0, 4, 6 and 8 g/L of PEG (from Sigma Aldrich, M_n = 4000 g/mol) were solved in each solution. The final solutions were stirred at 45 °C, 1000 rpm for 1 h to dissolve all constituents completely. After 24 h of aging, it was observed that the prepared solutions were stable. Glass slides were used as substrates which were ultrasonically cleaned in turn with detergent, nitric acid (1:4), acetone and ethanol for 10 min. To produce the CTS films, the prepared solutions were spin-coated onto glass substrates at 3000 rpm for 30 s followed by solvent-drying at 175 °C for 10 min on a hot plate. The spin-coating and solvent-drying processes were repeated five times to obtain the desired thickness of the films. Finally, the samples were put into a Pyrex tube containing a certain amount of sulphur powder. After evacuating to 5×10^{-4} mbar with a turbo pump, the tube was sealed with an oxygen/LPG weld. The samples were annealed under 1 atm of sulphur atmosphere for 2 h at 550 °C. The heating rate was 5 °C/min. After the annealing process, the samples were allowed to cool naturally to room temperature. The structural, morphological, compositional, optical and electrical properties of the samples were examined by XRD (PANalytical X'Pert PRO MPD with the wavelength of 1.5418 Å Cu Kα radiation), scanning electron microscopy (FEI, Quanta FEG 250), EDXS (Oxford Instruments ISIS 300), absorbance spectroscopy (UV–Visible spectroscopy, Thermo-Scientific, Evolution 60S) methods. Photo-transient current of the Ag/n–Si/CTS/Ag structures were obtained at 2 V under different illuminations of 50, 75 and 100 W/cm^2. The intensity of light was measured with a luxmeter (Testo-540). Resistance-temperature characteristics of the samples were investigated by two-point probe method in the temperature range of 300–473 K through a Keithley 6487 interfaced with computer by a Labview program.

3. Results and discussion

3.1. *Structural results*

The diffraction patterns were obtained at 40 keV operating voltage and 35 mA current. The step size and scan step time were 0.05° and 1 s, respectively. Figure 1 shows the obtained XRD patterns of the samples. From Figure 1, five peaks can be clearly seen at 2θ = 14.92°, 28.36°, 32.87°, 47.22° and 56.02° which are attributable to CTS (JCPDS 01-089-4714: Tetragonal, $a = b$ = 0.5413 nm, c = 1.0824 nm, I-42 m). The peaks

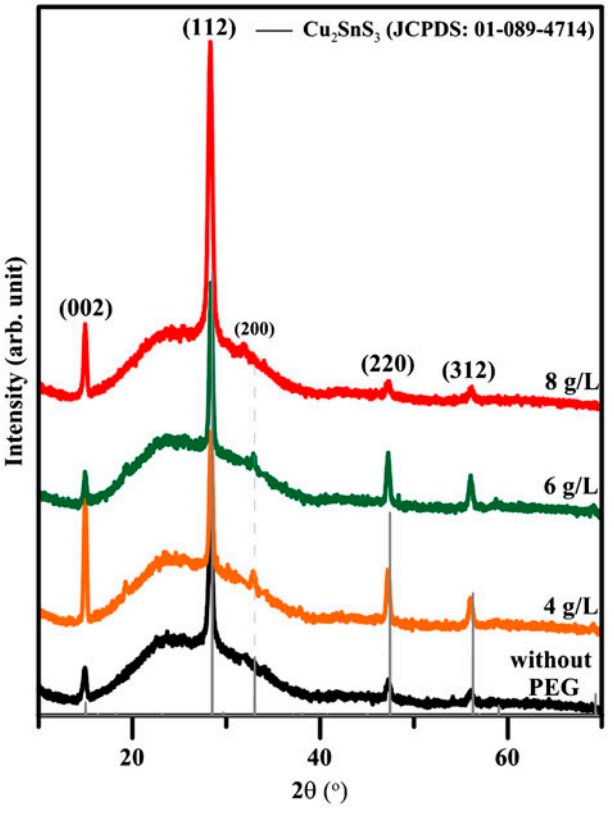

Figure 1. (colour online) Obtained X-ray diffraction patterns of the samples prepared with different PEG amounts.

correspond to (1 0 1), (1 1 2), (2 0 0), (2 2 0), (3 1 2) and (2 2 4) planes, respectively, and they indicate the polycrystalline nature of the films. The highest peak at 28.36° corresponding to (1 1 2) plane proves the preferred crystallization. No peak referring to other binary or ternary phases was detected in the patterns. As discussed in the experimental section, the XRD results support the idea that Cu-poor growth conditions may prevent the formation of secondary phases. As can be seen that the intensity of the peak corresponding to (1 1 2) plane increases with increasing PEG content. This means that PEG favours the growth of atomic planes along (1 1 2) direction under our experimental conditions. Similar trends on the enhancement of crystallization occurring with the addition of PEG were reported in literature. Vidyasagar et al. [37], investigated the effects of PEG concentration on the crystallinity of ZnO nanostructures. The XRD results revealed that particle size as well as crystallinity increases as the addition of the surfactant. Wang et al. [38] reported that the addition of PEG into the sol promotes the final crystallization of calcium phosphate glasses.

The average crystallite size of the films was calculated from the full width half maximum (FWHM) value of the peak (β), using the Debye–Scherrer equation [39]:

$$D = 0.94\lambda/\beta\cos\theta \quad (1)$$

where λ is the wavelength of X-ray radiation, θ is the Bragg angle of the peak and β is the angular width of the peak at FWHM. Each peak obtained in a diffractometer is broadened due to instrumental and physical factors (crystallite size and lattice strains) [40]. The microstrain (β) and dislocation density (ρ) for preferential orientation were calculated using the formulas given below [41]:

$$\varepsilon = \beta\cos\theta/4 \quad (2)$$

and

$$\rho = 15\varepsilon/aD \quad (3)$$

where a is the lattice constant. The estimations were done by taking into account all diffraction peaks and the obtained values are given in Table 1. According to Table 1, it can be seen that crystallite size of the films slightly increases with PEG concentration. As will be discussed in the photo-conversion measurement section, this trend suggests an improvement in photo-transient currents of the PEG-assisted growth of CTS films (Section 3.3).

3.2. *Morphological and compositional analysis*

Plain view SEM images of the samples prepared using different PEG amount are shown in Figure 2. The images reveal that the CTS films have continuous, dense and agglomeration-like morphology. It can be also seen that PEG-assisted grown films are composed of two different layers: one is a relatively smooth bottom-textured surface and the other one is randomly distributed with large particles on top surface. Through EDS studies, it was deduced that both layers consist of Cu, Sn and S, of which atomic percentages were consistent with Cu/Sn and S/metal ratios (Table 2). PEG is usually known as a polymeric binder as well as pore-forming agent. PEG-assisted deposits with porous structure usually resulted due to the nucleation and coalescence of small particles and the evaporation of PEG at elevated temperatures [34]. It was reported that porosity of the TiO_2 films increases with increasing PEG content due to high agglomeration of the particles on surface of the film [26]. Similarly, the agglomerated morphology of our samples may have resulted from the increasing PEG content.

EDXS analysis of the films is given in Table 2. It can be deduced that all obtained films have slightly Cu-poor composition. The Cu/Sn molar ratios are 1.90, 1.85, 1.82 and 1.86 for the films growth with 0, 4, 6 and 8 g/L, respectively, which are almost

Table 1. Estimated structural results of the samples.

Sample	Full width half maximum (radian)	Average crystallite size (nm)	Microstrain $x10^{-3}$	Dislocation density $x10^{-15}$ (m^{-2})
1 (0% wt. PEG)	0.473	18	2.00	3.06
2 (4% wt. PEG)	0.388	22	1.64	2.51
3 (6% wt. PEG)	0.386	22	1.63	2.49
4 (8% wt. PEG)	0.342	25	1.45	2.21

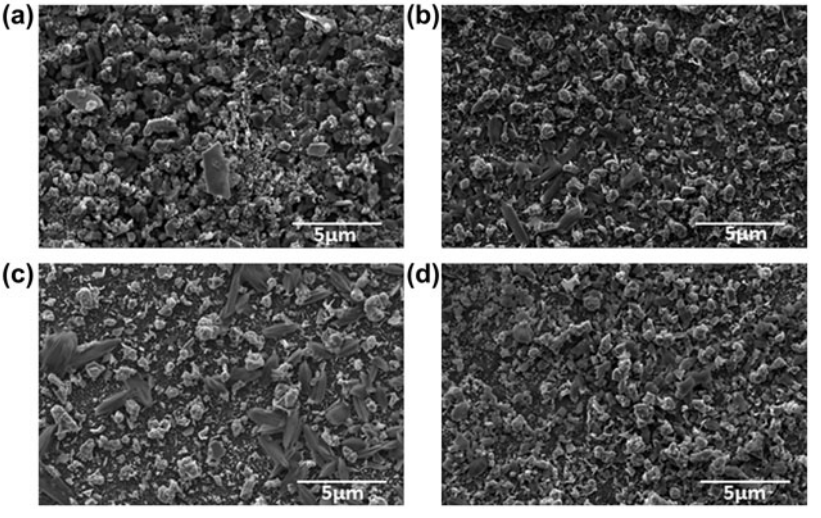

Figure 2. Plain view SEM images of the samples prepared using different PEG amounts.

Table 2. EDXS analysis of the films.

Sample	Cu	Sn	S	Cu/Sn	S/metal ion ratio
1 (0% wt. PEG)	31.94	16.81	51.25	1.90	1.05
2 (4% wt. PEG)	33.48	18.11	48.41	1.85	0.94
3 (6% wt. PEG)	31.93	17.52	50.55	1.82	1.02
4 (8% wt. PEG)	31.65	16.98	51.37	1.86	1.06

consistent with the initial ratio of precursor solution (Cu/Sn = 1.80). In addition, all films have S/metal ratios close to unity which indicate that sulphurization process was successfully completed. According to compositional results in Table 2, it can be also concluded that PEG content in starting solution doesn't change the composition of the CTS films.

3.3. *Photo-transient current characteristics of the Ag/n-Si/CTS/Ag structure*

To see the photo-conversion capability of the CTS films, n-Si/CTS hetero-junctions were also fabricated. Silver paste was used to get ohmic contact. The photo-transient current curves of the produced Ag/n-Si/CTS/Ag structure at 2.0 V under different illuminations are shown in Figure 3. As seen from Figure 3, the n-Si/CTS junctions exhibit good photo-conductivity and there is a sudden change in the photo-current. It is clear that the PEG-assisted grown samples show higher photo-conductivity than the sample grown without PEG. The I_{on}/I_{off} ratios for the junctions under different illuminations are given in Table 3. From Table 3, it can be seen that maximum I_{on}/I_{off} ratio was achieved for the sample grown with the assistance of 8 g/L of PEG. This behaviour confirms photo-sensitivity of the produced structure, suggests that PEG positively influences the photovoltaic conversion capability of the produced CTS films. Those

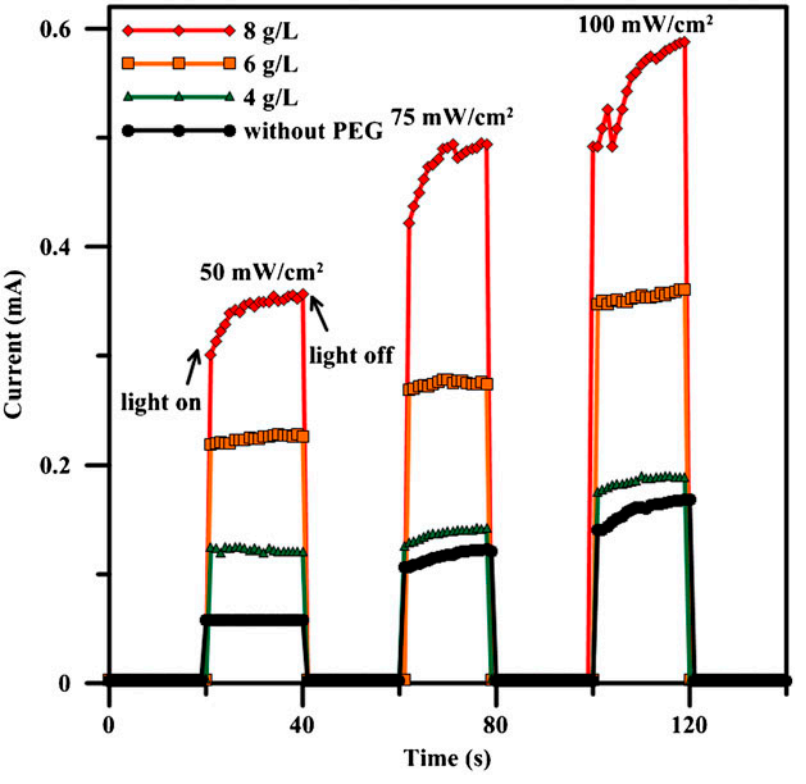

Figure 3. (colour online) The photo-transient current curves of the produced Ag/n-Si/CTS/Ag structure at 2.0 V under different illuminations.

Table 3. Electrical activation energies and light on/light off current ratios of the films under different illuminations.

	Electrical activation energy (meV)			I_{on}/I_{off}		
Sample	E_{A1}	E_{A2}	E_{A3}	50 mW/cm^2	75 mW/cm^2	100 mW/cm^2
Without PEG	13	93	363	21	45	61
4 g/L	21	131	403	46	54	72
6 g/L	69	132	278	84	106	139
8 g/L	31	90	359	116	189	225

relatively low photocurrents may be due to lower agglomeration occurring on the film surface which resulted from the PEG-assisted growth. A similar observation was also reported in literature [26].

3.4. *Electrical results*

To identify the majority carrier type of the films, the thermo–emf method was used [42]. The samples exhibited p-type semiconductor nature thereby the majority carriers

were holes. In order to find impurity levels' electrical activation energies, resistivity-temperature behaviour of the samples was investigated in the temperature range of 300–473 K. Silver paste was painted on the surface of films to achieve ohmic contact. Theoretical background of the method, which we made use of to find impurity levels' electrical activation energies, can be summarized as below:

Based on the solid-state theory of semiconductors [43,44], in the case of a semiconductor with one or more impurity levels, the relation between dark electrical resistance of a film and temperature is given by

$$R(T) = R_0 e^{E_g/2kT} + \sum_{i=1}^{n} R'_{0,i} e^{\Delta E_i/kT} \tag{4}$$

In Equation (4), R_0 and $R'_{0,i}$ are constants, E_g is the thermal band gap energy, ΔE_i is the electrical activation energies of the impurity levels, k is Boltzmann's constant and T is temperature. The overall conductivity of the semiconductor samples is dominated by the charge carriers generated by ionization of impurity levels (extrinsic conductivity) in a relatively low temperature, and thus the second term in Equation (4) governs the R_T value. At relatively higher temperatures, the temperature dependence of conductivity is dominated by the band-to-band electronic transitions. The charge carriers acquire enough thermal energy to make an inter-band transition (the intrinsic conductivity is "activated" at these temperatures) under certain conditions [43]. According to the discussion above, the two terms appearing in Equation (4) may be used independently in the corresponding temperature intervals. So in the graph of ln(R) vs. 1000/T, a number of linear trends appear which indicate a number of impurity levels. Thus, the second term in Equation (4) prevails in the R_T dependence in the studied temperature interval (300–473 K). The decrease in dark electrical resistance upon increase in temperature in the region of extrinsic conductivity (corresponding to the lower temperature interval) follows the equation:

$$R(T) = \sum_{i=1}^{n} R'_{0,i} e^{\Delta E_i/kT} \tag{5}$$

Figure 4 shows ln(R) vs. 1000/T graphs of the samples. The presence of discrete linear regions in Figure 4 suggests that there are two types of conduction mechanisms present in the studied samples. Using Equation (5), ΔE can be easily written as

$$\Delta E = k \frac{\mathrm{d}(\ln R(T))}{\mathrm{d}(1/T)} \tag{6}$$

Electrical activation energy values of the impurity levels were estimated from the slopes of ln(R) vs. 1000/T graphs. Three values were estimated for each film and are summarized in Table 3. Impurity level electrical activation energy (ΔE) values of the thin film samples were found in between 13 and 403 meV for samples grown with or without PEG. There are two studies reporting the electrical activation energies for CTS thin films in literature. Bouazizet al. [18] reported CTS thin films synthesized by solid-state reaction method and found 25 meV in a temperature interval of 90–300 K. Kahraman et al. [45] reported electrical activation energies for chemically grown CTS thin films between 40 and 130 meV in 300–723 K.

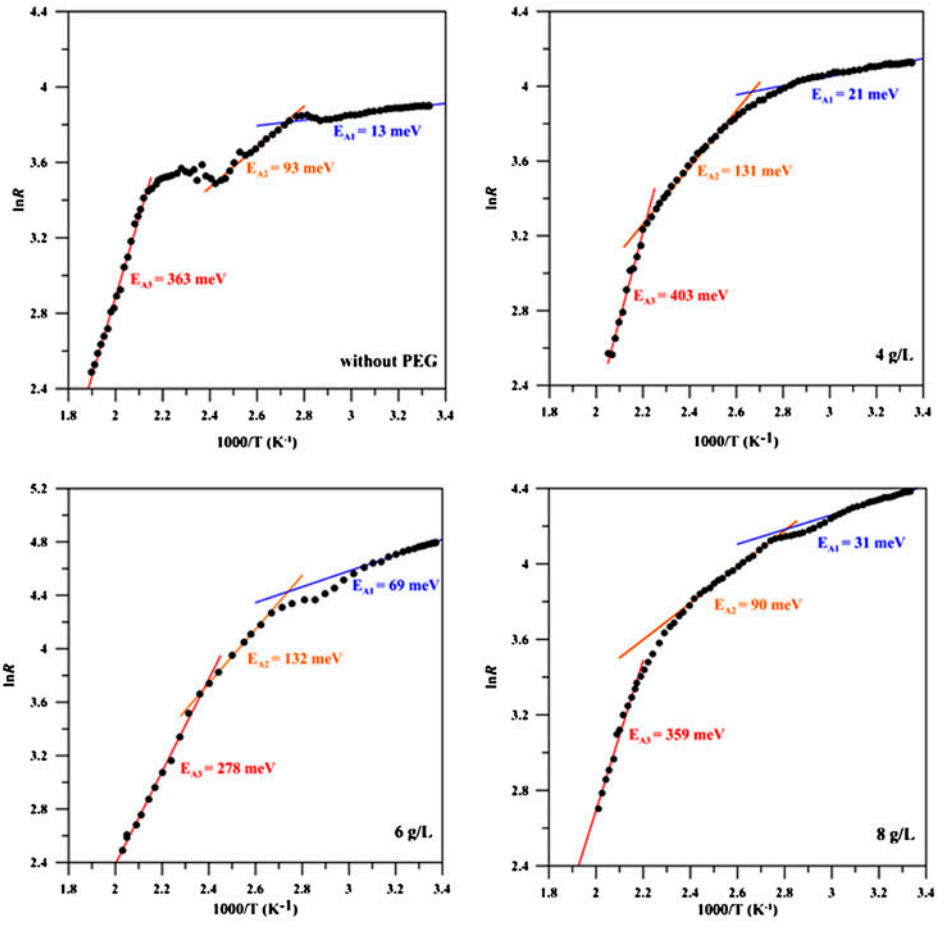

Figure 4. (colour online) ln(R) vs. 1000/T graphs of the samples prepared with different PEG amounts.

3.5. *Optical results*

Near the absorption edge or in the strong absorption zone of the transmittance spectra, the absorption coefficient is related to the optical energy gap, E_g following the power-law behaviour of Tauc's relation [46,47].

$$(\alpha h\nu) = B(h\nu - E_g)^m \tag{7}$$

where B is an energy-independent constant, E_g is the optical band gap energy and m is an index that characterizes the optical absorption process and is theoretically equal to 2 and 1/2 for indirect- and direct-allowed transitions, respectively. Figure 5 shows the band gap photon energy estimations performed via extrapolating the linear region of the plot $(\alpha h\nu)^2$ vs. $(h\nu)$ to the horizontal axis and considering the intersecting point. As can be seen from Figure 5, the samples exhibit linear dependence which indicates directly the transition nature of the films. Thus, we can choose m as 1/2. By plotting the graph

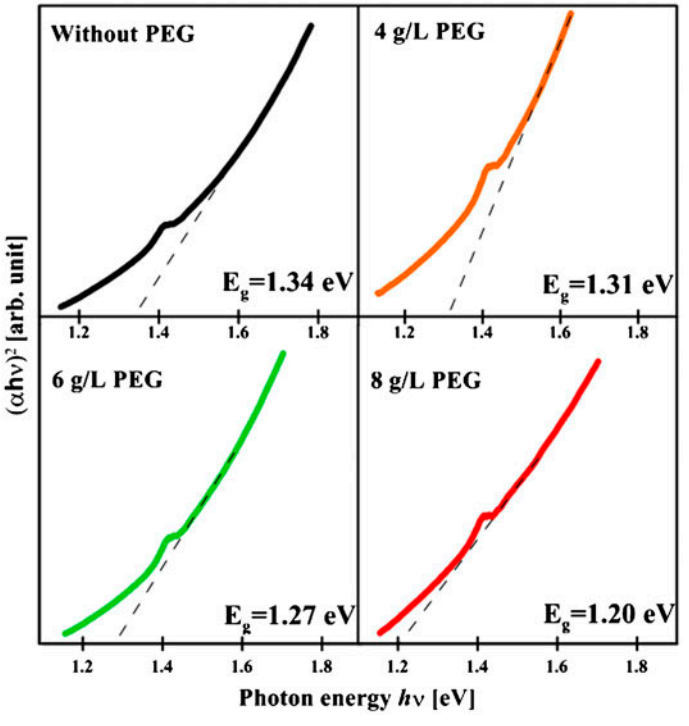

Figure 5. (colour online) The plots of $(\alpha hv)^2$ vs. photon energy hv of the samples prepared with different PEG amounts.

of $(\alpha hv)^2$ against photon energy (hv), the band gap values were estimated as 1.34, 1.31, 1.27 and 1.20 eV for the samples with 0, 4, 6 and 8 g/L PEG, respectively. As a p-type direct band gap semiconductor, its band gap energy varies depending on the type of crystal structure and has been reported in between 0.93 and 1.51 eV [17,19,48]. The reason for the difference between the reported values depends on the crystal structure of polymorphic compound CTS, where 0.98 eV was measured for a cubic phase and 1.35 eV for a tetragonal phase [19]. The polymorphic state of grown CTS depends on the growing temperature, where the cubic phase is known to form at high temperatures (>775 °C) and the monoclinic and triclinic as well as the tetragonal phases are low-temperature phases (<775 °C) [17,49]. It can be said that the estimated results decrease with increasing PEG amount and are in good agreement with literature values. Such band gap values found in the present study are quite close to the optimum band gap for a solar cell, which make the films promising absorber materials.

4. Conclusions

In this study, PEG-assisted growth of CTS thin films has been achieved, for the first time, by using sol–gel spin-coating method. A structural improvement and an increase in crystallite size were observed with increasing PEG content. This trend provided a significant improvement in photovoltaic behaviour of the CTS films. A remarkable

agglomeration occurred with increasing PEG content. Impurity level electrical activation energies were found through resistivity-temperature characteristics of different conduction mechanisms. Optical band gap values of the films decreased with increasing PEG content. Finally, it has been shown that PEG-assisted growth of CTS thin films is a promising way to improve its photovoltaic characteristics.

Acknowledgements

The financial support from Scientific Research Commission of the Mustafa Kemal University (Project No: 11,680) is greatly appreciated.

References

[1] S. Emin, S.P. Singh, L. Han, N. Satoh and A. Islam, Sol. Energy 85 (2011) p.1264.
[2] S. Blöb and M. Jansen, Z. Naturforsch 58b (2002) p.1075.
[3] X. Liang, Q. Cai, W. Xiang, Z. Chen, J. Zhong, Y. Wang, M. Shao and Z. Li, J. Mater. Sci. Technol. 29 (2013) p.231.
[4] B. Qu, H. Li, M. Zhang, L. Mei, L. Chen, Y. Wang, Q. Li and T. Wang, Nanoscale 3 (2011) p.4389.
[5] B. Qu, M. Zhang, D. Lei, Y. Zeng, Y. Chen, L. Chen, Q. Li, Y. Wang and T. Wang, Nanoscale 3 (2011) p.3646.
[6] M. Ristov, G. Sinadinovski, M. Mitreski and M. Ristova, Sol. Energy Mater. Sol. Cells 69 (2001) p.17.
[7] Z. Su, K. Sun, Z. Han, F. Liu, Y. Lai, J. Li and Y. Liu, J. Mater. Chem. 22 (2012) p.16346.
[8] J. Koike, K. Chino, N. Aihara, H. Araki, R. Nakamura, K. Jimbo and H.Katagiri, Jpn. J. Appl. Phys. 51 (2012) p.10NC34.
[9] D. Avellaneda, M.T.S. Nair and P.K. Nair, J. Electrochem. Soc. 157 (2010) p.D346.
[10] D. Tiwari, T.K. Chaudhuri, T. Shripathi and U. Deshpande, AIP Conf. Proc. 1447 (2012) p.1039.
[11] K. Chino, J. Koike, S. Eguchi, H. Araki, R. Nakamura, K. Jimbo and H. Katagiri, Jpn. J. Appl. Phys.51 (2012) p.10NC35.
[12] V.A. Kovalenker, V.S. Malov, T.L. Yevstigneyeva and L.N. Vyalsov, Int. Geol. Rev. 25 (1983) p.117.
[13] T.A. Kuku and O.A. Fakolujo, Sol. Energy Mater. 16 (1987) p.199.
[14] M. Bouaziz, M. Amlouk and S. Belgacem, Thin Solid Films 517 (2009) p.2527.
[15] D. Wu, C.R. Knowles and L.L.Y. Chang, Miner. Mag. 50 (1986) p.323.
[16] X. Chen, H. Wada, A. Sato and M. Mieno, J. Solid State Chem. 139 (1998) p.144.
[17] M. Onoda, X. Chen, A. Sato and H. Wada, Mater. Res. Bull. 35 (2000) p.1563.
[18] M. Bouaziz, J. Ouerfelli, S. Srivastava, J. Bernède and M. Amlouk, Vacuum 85 (2011) p.783.
[19] P. Fernandes, P. Salomé and A. Cunha, J. Phys. D: Appl. Phys. 43 (2010) p.215403.
[20] P.A. Fernandes, P.M.P. Salomé, A.F. and da Cunha, J. Alloys Compd. 509 (2011) p.7600.
[21] Q. Chen, X. Dou, Y. Ni, S. Cheng and S. Zhuang, J. Colloid Interface Sci. 376 (2012) p.327.
[22] B. Li, Y. Xie, J. Huang and Y. Qian, J. Solid State Chem. 153 (2000) p.170.
[23] A. Amlouk, K. Boubaker and M. Amlouk, Vacuum 85 (2010) p.60.
[24] C.X. Li, J. Guo, D.Y. Jiang and Q. Li, Adv. Mater. Res. 624 (2012) p.59.
[25] H. Dahman, S. Rabaoui, A. Alyamani and L. El Mir, Vacuum 101 (2014) p.208.
[26] M. Md. Rahman, H. Tanaka, T. Soga, T. Jimbo and M. Umenot, *Photovoltaic Specialists Conference*, in *2000 Conference Record of the Twenty-Eighth IEEE*, 2000, p.806.

[27] M. Mouanga, L. Ricq, G. Douglade, J. Douglade and P. Berçot, Surf. Coat. Tech. 201 (2006) p.762.
[28] Y. Zhu, Y. Chen and L. Liu, J. Cryst. Growth. 328 (2011) p.70.
[29] K.H. Park and C.K. Hong, Electrochem. Commun. 10 (2008) p.1187.
[30] J. Wan, Y. Lei, Y. Zhang, Y. Leng and J. Liu, Electrochim. Acta 59 (2012) p.75.
[31] Z. Hua, Z. Xing-Zhong, Y. Bing-Chu, Z. Dou, L. Zhi-You and Z. Ke-Chao, J. Colloid Interface Sci. 374 (2012) p.9.
[32] S. Fan, C. Li, C. Li, G. Liu, G. Yang and L. Zhang, Mater. Trans. 47 (2006) p.1703.
[33] T. Pradubsang, T. Amornsakchai and U. Asawapirom, J. Microsc. Soc. Thailand 4 (2011) p.130.
[34] T.S. Senthil and M. Kang, Bull. Korean Chem. Soc. 34 (2013) p.1188.
[35] A.I. Maldonado-Valdivia, E.G. Galindo, M.J. Ariza and M.J. García-Salinas, Sol. Energy 91 (2013) p.263.
[36] S. Chen, X.G. Gong, A. Walsh and S. Wei, Appl. Phys. Lett. 96 (2010) p.021902.
[37] C.C. Vidyasagar and Y. Arthoba Naik, Arab. J. Chem. doi: 10.1016/j.arabjc.2012.08.002.
[38] X. Wang, S. Cai, T. Liu, M. Ren, K. Huang, R. Zhang and H. Zhao, Ceram. Int. 40 (2014) p.3389.
[39] G. Knuyt, C. Quaeyhaegens, J. D'Haen and L.M. Stals, Phys. Status Solidi B 195 (1996) p.179.
[40] H.P. Klug and L. Alexander, *X-ray Diffraction Procedures for Polycrystalline and Amorphous Materials*, John Wiley, New York, 1974.
[41] A. Suresh, K. Chatterjee, V.K. Sharma, S. Ganguly, K. Kargupta and D. Banerjee, J. Elect. Mater. 38 (2009) p.449.
[42] K. Seeger, *SemiconductorPhysics*, Springer, Berlin, 1973.
[43] B. Pejova, A. Tanuševski and I. Grozdanov, J. SolidStateChem. 178 (2005) p.1786.
[44] S. Kahraman, M. Podlogar, S. Bernik and H.S. Güder, Metall. Mater. Trans. A 45 (2014) p.2326.
[45] S. Kahraman, S. Çetinkaya, H.M. Çakmak, H.A. Çetinkara and H.S. Güder, Int. J. Mater. Res. 104 (2013) p.1020.
[46] J. Tauc, Mater. Res. Bull. 5 (1970) p.721.
[47] S. Sönmezoğlu, A. Arslan, T. Serin and N. Serin, Phys. Scr. 84 (2011) p.065602.
[48] M. Bouaziz, M. Amlouk and S. Belgacem, Thin Solid Films 517 (2009) p.2527.
[49] A.C. Rastogi and S. Salkalachen, Thin Solid Films 97 (1982) p.191.